

1 **Enhanced understanding of dominant drivers of**
2 **Water Yield change across China through the**
3 **improved coupled carbon and water model**

4 Huilan Shen ^{1,2}, Hanbo Yang ^{1,2,*}, Changming Li ^{1,2,3}

5 ¹ Department of Hydraulic Engineering, Tsinghua University, Beijing 100084, China

6 ² State Key Laboratory of Hydrosience and Engineering, Tsinghua University, Beijing 100084, China

7 ³ School of Civil Engineering and Transportation, State Key Laboratory of Subtropical Building and
8 Urban Science, South China University of Technology, Guangzhou 510641, China

9 * Correspondence: Hanbo Yang (yanghanbo@tsinghua.edu.cn)

10

11

12 **Abstract:** The rapid environmental changes, including climate change, escalating
13 atmospheric CO₂ concentration ([CO₂]), and vegetation dynamics, have been
14 significantly impacting hydrological processes. Yet disentangling the respective
15 contributions of climate, vegetation, and [CO₂] change to water yield (WY)—
16 especially clarifying [CO₂]-driven physiological effects—remains difficult. Therefore,
17 this study improved the coupled carbon and water (CCW) model by integrating
18 dynamic water-use efficiency (WUE) to better capture [CO₂] physiological
19 feedbacks.~~Therefore, this study improved the coupled carbon and water (CCW) model~~
20 ~~integrating dynamic water use efficiency (WUE) better capture CO₂ physiological~~
21 ~~feedbacks.;~~ Using scenario analysis, WY changes across China from 1982 to 2017 were
22 attributed to climate, vegetation, and [CO₂] drivers. The results showed that climate
23 change (especially precipitation change) emerged as the dominant driver, directly
24 affecting over 70% of China's land area. The vegetation change was the second largest
25 factor to reduce WY, especially in central China. The effect of the escalating [CO₂] was
26 relatively small. Spatial analysis aligned with isohyetal lines further revealed that
27 vegetation change and [CO₂] exerted greater influence within the 400–1600 mm
28 precipitation range. In addition, the elasticity analysis showed that the sensitivity
29 ranking of impact factors is precipitation > [CO₂] > NDVI for the whole China.
30 Therefore, CMIP6 SSP585 projections indicate that accelerating [CO₂] rise will
31 amplify its hydrological effect to a +1.29% annual WY increase by 2100, surpassing
32 vegetation influences, implying a stronger hydrological role under future forcing. By
33 explicitly representing dynamic WUE, this study improves process-based WY
34 attribution and shows that [CO₂] physiological regulation can partly offset vegetation-
35 induced WY reductions.~~This study refines WY attribution by coupling dynamic WUE~~
36 ~~with ecohydrological modeling-, thereby providing new insights for regional water~~
37 ~~resource management under climate change.~~valuable insights for optimizing regional
38 water resource allocation and developing adaptive ecosystem management strategies
39 under future climate scenarios.

40 **Keywords:** the coupled carbon and water (CCW) model; WY change; climate change;
41 vegetation change; increasing atmospheric CO₂ concentrations; attribution analysis

42 **Plain language:** Climate change, rising CO₂, and vegetation dynamics are reshaping
43 global water cycle, but their impacts remain unclear. We improved the coupled carbon
44 and water model to analyze China's water yield (~~WY~~) changes (1982–2017). Our
45 results showed that climate change was the dominant driver nationally, vegetation/ CO₂
46 most affected in 400-1600 mm precipitation zones. Projections indicate CO₂ may
47 increase WY 1.3% annually by 2100, surpassing other drivers. This work informs
48 sustainable water management.

49 1 Introduction

50 The global environment has been undergoing rapid changes, impacting
51 hydrological processes through climate change, escalating atmospheric CO₂
52 concentration [CO₂], and vegetation dynamics (Piao et al., 2007; Wei et al., 2024).
53 Notably, China has experienced a visible greening trend in recent decades, prompting
54 a heightened focus on ecological and water resource concerns (Chen et al., 2019).
55 Investigating the influence of vegetation changes on runoff has thus emerged as a
56 pivotal research area, aligning with China's increasing emphasis on environmental
57 sustainability. Among hydrological metrics, water yield (WY) is especially relevant
58 because it directly represents the amount of water remaining after evapotranspiration
59 and is therefore closely linked to runoff generation and regional water availability.
60 China's diverse climatic zones and pronounced greening make it an ideal natural
61 laboratory for investigating these ecohydrological feedbacks, with implications for both
62 China ~~China's diverse climatic zones and pronounced greening make it an ideal natural~~
63 ~~laboratory for investigating these ecohydrological feedbacks, with insights that are~~
64 ~~globally relevant yet directly informative for sustainable water resource management~~
65 ~~and ecological restoration in China~~(Ogotu et al., 2021; Yang et al., 2019); -and other
66 semi-arid and monsoon-influenced regions such as the Sahel, South Asia, and the
67 Mediterranean Basin ~~and for other semi-arid and monsoon-influenced regions such as~~
68 ~~the Sahel, South Asia, and the Mediterranean Basin~~(Nkiaka et al., 2025; Rahman et al.,
69 2025; Serrano-Notivoli et al., 2022). Understanding how vegetation dynamics, climate
70 change, and [CO₂] interact to regulate WY is therefore of both scientific and practical
71 importance for water resource management and ecological restoration under
72 accelerating environmental change.~~Understanding the intricate interplay among~~
73 ~~vegetation dynamics, climate change, and [CO₂] within the water cycle, particularly~~
74 ~~concerning runoff therefore it is not only of global relevance but also of profound~~
75 ~~importance for advancing sustainable water resource management and ecological~~
76 ~~restoration strategies in China under accelerating environmental change~~

77 Several methods have been employed to separate the effects of climate, vegetation,
78 and [CO₂] change on runoff change, including paired catchment experiments, statistical
79 methods, and modeling approaches (Zeng et al., 2020). Given that annual water yield
80 (WY) equates to runoff through negligible soil water storage changes, these
81 methodological evaluations directly inform WY attribution frameworks (Zhang et al.,
82 2022b). The paired catchment experiment method, though classical, is limited to small-
83 scale watersheds and is less applicable to larger regions (Peng et al., 2016). Statistical
84 methods, while helpful in identifying correlations, lack a physical basis and are
85 insufficient for explaining the underlying mechanisms of runoff changes (Chen et al.,
86 2022). Modeling approaches for attribution fall into two broad classes: (i) process-
87 based models that explicitly simulate coupled water–energy–carbon processes, and (ii)
88 conceptual models that approximate these processes with parsimonious, physically
89 interpretable relationships (Zhai and Tao, 2021). Process-based models can capture
90 detailed mechanisms, but they require extensive inputs and many parameters, are
91 sensitive to calibration and equifinality, and are computationally demanding—
92 limitations that hinder basin-to-continental applications over long periods (Jiao et al.,
93 2017; Ma et al., 2023). By contrast, conceptual models retain key ecohydrological
94 mechanisms with far fewer parameters, scale well to large regions, and thus are well
95 suited for large-scale attribution while preserving physical interpretability. Among
96 these conceptual models, the Budyko framework, widely used to separate climate
97 change effects on runoff, quantifies water balance through the aridity index
98 (PET/precipitation) and incorporates a catchment-specific Budyko parameter (“n”²)
99 representing integrated land surface characteristics (e.g., vegetation, soil, topography)
100 (Zhang et al., 2022a, 2016a). However, most Budyko-based applications primarily
101 emphasize climate-driven attribution; vegetation and [CO₂] influences are typically
102 introduced only indirectly—by assigning temporal changes in the Budyko parameter
103 (“n”²)—to vegetation (Tan et al., 2024; Xue et al., 2022; Zhou et al., 2023) or correlating
104 the Budyko parameter (n) “n”² with NDVI (Liu et al., 2024; Tan et al., 2023), and by

105 embedding [CO₂] effects through PET adjustments(Liu et al., 2024). —These practices
106 conflate vegetation with other controls captured by- the Budyko parameter (n)^{“n”} (e.g.,
107 soil, topography) and mix [CO₂]-physiological impacts with meteorological drivers in
108 PET, making it difficult to isolate vegetation structural change from [CO₂]-induced
109 stomatal adjustments and to ascribe mechanisms robustly (Gan et al., 2021).

110 Specifically, elevated [CO₂] reduces stomatal conductance—due to smaller
111 stomatal apertures and increased leaf resistance (Lammertsma et al., 2011; Xu et al.,
112 2016) which decreases transpiration fluxes (ET). At the same time, carbon assimilation
113 rate (GPP) may increase with higher [CO₂] availability, but this increase is often less
114 proportional to the reduction in water loss (Montibeller et al., 2022) The resulting
115 imbalance—lower water loss relative to carbon gain—thus leads to higher water-use
116 efficiency (WUE = GPP / ET). In particular, conventional frameworks that neglect
117 [CO₂]-driven physiological feedbacks fail to represent the enhanced water-use
118 efficiency (WUE) of vegetation under elevated [CO₂] conditions. This omission leads
119 to ambiguous attribution of runoff variations, as part of the reduction in
120 evapotranspiration induced by stomatal closure is often misinterpreted as a vegetation
121 structural effect rather than a [CO₂]-induced physiological adjustment. Although
122 numerous studies have examined vegetation and climate controls on runoff, few have
123 explicitly incorporated the [CO₂]-WUE feedback within a mechanistic framework.
124 Most existing approaches either completely ignore this feedback or treat it as a simple
125 empirical or linear relationship, rather than capturing its process-based influence on
126 hydrological responses.

127 The coupled carbon and water (CCW) model integrates hydrological and
128 ecological processes by mechanistically linking vegetation dynamics to water and
129 carbon fluxes through remote sensing-driven parameterization (Li et al., 2024b; Zhang
130 et al., 2021b, 2022b). Unlike the Budyko framework’s empirical parameter “n”—which
131 conflates vegetation effects with unaccounted catchment characteristics—the CCW
132 model links vegetation and hydrology through a single mechanistic chain. In this

133 framework, vegetation structure (NDVI/LAI) determines canopy absorption of
134 photosynthetically active radiation (FPAR) and hence gross primary production (GPP)
135 via light-use efficiency, while evapotranspiration (ET) is coupled to GPP through a
136 biome-specific underlying water-use efficiency (UWUE) term with vapor pressure
137 deficit (VPD) regulation. Nevertheless, the original CCW model, while robust in
138 capturing vegetation-climate interactions, adopts a static UWUE and does not account
139 for CO₂-induced physiological changes, specifically long-term enhancements in water-
140 use efficiency (WUE) resulting from elevated [CO₂], thereby limiting its capacity to
141 isolate [CO₂] fertilization effects from vegetation structural and climatic influences
142 (Adams et al., 2020; Li et al., 2023).

143 To address this limitation, our study enhanced the CCW framework by
144 incorporating dynamic WUE responses to [CO₂], allowing explicit attribution of runoff
145 changes to three distinct drivers—climate change (eg. precipitation, temperature, and
146 so on), vegetation structural change (NDVI, and land use and land cover (LULC)), and
147 [CO₂]-physiological effects (stomatal optimization). This extension advances beyond
148 empirical or regression-based attribution, clarifies how [CO₂] modulates vegetation–
149 hydrology interactions across large spatial scales, and provides policy-relevant
150 evidence for sustainable water resource management and ecological restoration in
151 China under accelerating environmental change. .

152 **2 Methods and Data**

153 **2.1 Data sources and processing**

154 Four main datasets were employed in the improved CCW model: vegetation data
155 (NDVI), climate data (precipitation, temperature, shortwave radiation, vapor pressure
156 deficit, and atmospheric pressure), land use and land cover (LULC), and [CO₂]. The
157 monthly NDVI dataset used in this study (Table 1) was derived from a daily 0.05° gap-
158 free NDVI dataset in China (<https://doi.org/10.6084/m9.figshare.c.7002225.v1>) (Li et
159 al., 2024a), which was developed from the NOAA’s daily NDVI dataset, applying

160 effective data recognition and spatiotemporal gap-filling techniques. The dataset spans
161 1981–2023 and provides a spatial resolution of 0.05° , and we used bilinear interpolation
162 to generate the dataset with a spatial resolution of 0.1° .

163 Climate data (Table 1), including precipitation, air temperature, surface downward
164 shortwave radiation, relative humidity, and atmospheric pressure, were sourced from
165 the China Meteorological Forcing Dataset (CMFD) at the National Tibetan Plateau
166 Data Center (TPDC) of the Institute of Tibetan Plateau Research, Chinese Academy of
167 Sciences (He et al., 2020). The dataset spans 1979–2018 and provides a spatial
168 resolution of 0.1° and temporal resolutions at 3-hour, daily, monthly, and annual scales.
169 As the dataset did not provide vapor pressure deficit (VPD), we calculated VPD using
170 the method from Howell and Dusek (1995), based on atmospheric pressure, temperature,
171 and relative humidity.

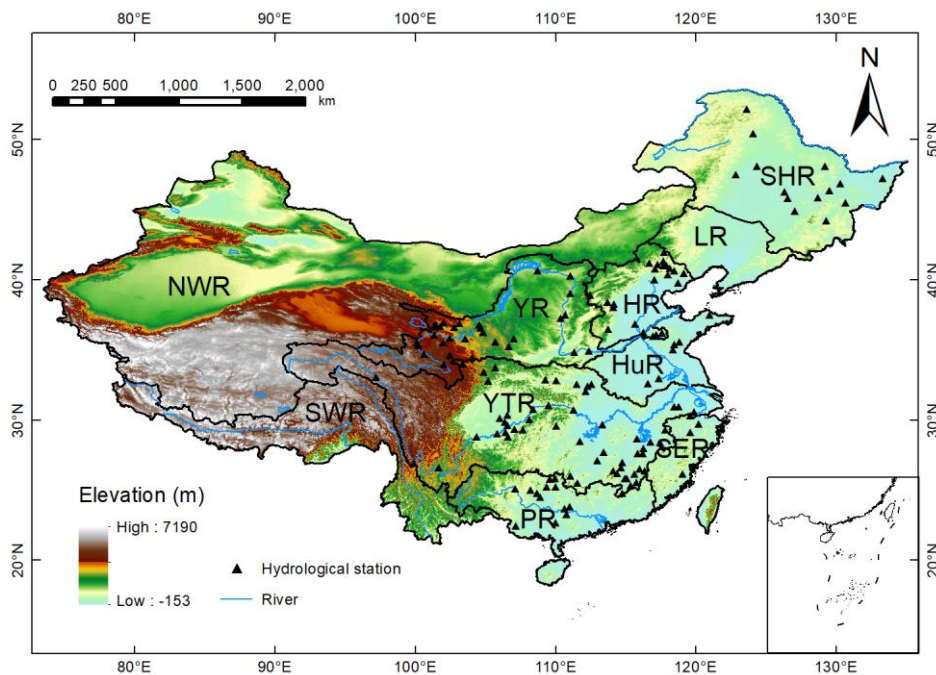
172 LULC data (Table 1) were obtained from the Zhang et al. (2024) global dataset,
173 which provides consistent multi-temporal global LULC maps at 30 m spatial resolution
174 for 1985–2022. The dataset includes 35 fine-resolution LULC types. For the purposes
175 of this study, and to facilitate LULC change analysis, we merged these 35 LULC types
176 into 17 types using the IGBP classification, based on the method by Yang et al. (2017).
177 Four primary LULC types—cropland, forest, grassland, and bare land—were
178 determined following the method described by Mu et al. (2013). The data were
179 resampled to the 0.1° spatial resolution, ensuring compatibility for modeling within the
180 modified CCW framework.

181 $[\text{CO}_2]$ data were sourced from the Mauna Loa Observatory (MLO), Hawaii (20°N ,
182 156°W) (<http://cdiac.esd.ornl.gov/ftp/trends/co2/maunaloa.co2>), with yearly
183 observations used to represent national $[\text{CO}_2]$ levels due to the minimal spatial variation
184 in $[\text{CO}_2]$ across China (Table 1). These datasets were then used to drive the improved
185 CCW model.

186 In this study, the hydrological data for model validation from 145 hydrological
 187 stations (Fig. 1), each with at least 15 years of continuous data since 1982, was collected
 188 from the Hydrological Bureau of the Ministry of Water Resources of China
 189 (<https://www.mwr.gov.cn/english/>). Annual runoff data were calculated from the daily
 190 runoff and the catchment area controlled by each hydrological station.

191 **Table 1.** Hydrology, climate, and vegetation data for the improved CCW model

Dataset	Original Resolution (spatial/temporal)	Period	Reference
NDVI	0.05° × 0.05° (daily)	1981 - 2023	(Li et al., 2024a)
Landcover	30m×30m (5-year)	1985 - 2022	(Zhang et al., 2024)
Climate	0.1° × 0.1° (monthly)	1979 - 2018	(He et al., 2020)
[CO ₂]	yearly	1959 - 2023	Mauna Loa Observatory, Hawaii
Streamflow	daily	1982 - 1995 (or later)	On-site streamflow records and the regional flow summary reports of government



192

193 **Figure 1.** The geographic location and topography of the study area, where the black triangles
 194 mark the location of the hydrological gauging stations for model evaluation. Ten river basins
 195 considered in this study are: Songhua River basin (SHR), Liao River basin (LR), Hai River
 196 basin (HR), Huai River basin (HuR), Yangtze River basin (YZR), Yellow River basin (YR),
 197 Pearl River basin (PR), Southeast Rivers (SER), Southwest Rivers (SWR) and Northwest
 198 Rivers (NWR).

199 **2.2 The improved CCW model**

200 The original Coupled Carbon and Water (CCW) model (Zhang et al., 2016b) is a
201 data-driven, remote sensing-based model that effectively integrates carbon and water
202 dynamics to estimate monthly gross primary productivity (GPP) and evapotranspiration
203 (ET). This model, which is particularly carbon-centric, derives ET from GPP
204 constrained by underlying water-use efficiency (UWUE) parameters, which were
205 calibrated using global FLUXNET data (Zhang et al., 2016b; Zhou et al., 2014). Despite
206 its simpler structure, the CCW model achieves accuracy comparable to more complex
207 process-based models in ET estimation. The essential components of the CCW model
208 are represented as:

$$209 \quad GPP = APAR \times \varepsilon = PAR \times FPAR \times \varepsilon_{pot} \times R_s \times T_s \times W_s \quad (1)$$

210 where APAR is the absorbed photosynthetically active radiation (MJ m^{-2}), which is
211 calculated as the product of incident photosynthetically active radiation (PAR) and the
212 fraction of PAR absorbed by vegetation (FPAR), and PAR is typically assumed to be
213 45% of the total shortwave radiation (Running et al., 2000); FPAR is determined by the
214 normalized difference vegetation index (NDVI) (Sims et al., 2005); ε is the realized
215 light-use efficiency (g C MJ^{-1}), which is calculated by multiplying the potential light-
216 use efficiency (ε_{pot}) and environmental scalars for diffuse radiation (R_s), temperature
217 (T_s), and moisture stress (W_s). This formulation ensures that GPP estimates reflect the
218 influence of radiation, temperature, and moisture limitations on photosynthetic activity.

219 In this study, we improve the CCW model by incorporating dynamic water use
220 efficiency (WUE) instead of static UWUE. This enhancement addresses the limitations
221 of the original model, particularly its inability to adapt to environmental changes such
222 as varying $[\text{CO}_2]$ and vapor pressure deficit (VPD). WUE's estimation method is
223 estimated using the WEC (Water Efficiency and Carbon) equation proposed by Cheng
224 et al. (2017), where WUE is defined at the ecosystem scale as the ratio of GPP to total
225 ecosystem evapotranspiration rather than as a leaf-level intrinsic WUE. Under this

226 framework, evapotranspiration includes transpiration, soil evaporation, and canopy
 227 interception, and the analytical upscaling from stomatal theory to ecosystem WUE is
 228 represented through the transpiration–soil evaporation partitioning term and the
 229 interception term. The final formula for calculating WUE is:

$$230 \quad WUE = \frac{C_a \times P_a}{1.6(VPD + g_1\sqrt{VPD})} [1 - \exp(-k * LAI)](1 - f_i) \quad (2)$$

231 where C_a is atmospheric CO₂ concentration (mol(CO₂) mol⁻¹(air)); P_a is atmospheric
 232 pressure (kPa); VPD is vapor pressure deficit (kPa); g_1 is an empirical parameter of the
 233 Ball stomatal conductance model; k is the radiation extinction coefficient, typically set
 234 at 0.6, describing how light is absorbed by the canopy; LAI is the leaf area index; and
 235 f_i is a factor representing nonproductive water use (such as evaporation from soil and
 236 canopy interception). This equation provides a dynamic estimate of WUE, considering
 237 the effects of environmental factors like VPD, CO₂ concentration, atmospheric pressure,
 238 and canopy structure (LAI). The factor $1 - \exp(-k \times LAI)$ represents the partitioning
 239 between transpiration and soil evaporation associated with canopy cover at monthly-
 240 to-annual scales~~accounts for light interception by the canopy~~. In this study, the
 241 interception evaporation factor (f_i) was set to zero to reduce data requirements and
 242 maintain consistency in long-term grid-scale attribution. This simplification follows
 243 previous large-scale ecohydrological studies (Cheng et al., 2017), which reported that
 244 canopy interception and soil surface evaporation account for a minor portion of total
 245 evapotranspiration at annual to multi-decadal scales. Given that the improved CCW
 246 model focused on yearly water yield (WY) dynamics rather than event-scale
 247 hydrological responses, neglecting interception loss reduces model complexity without
 248 substantially affecting WY estimation.

249 In order to ensure the consistency of NDVI and LAI trends, we calculated LAI
 250 using NDVI (Gutman and Ignatov, 1998) instead of LAI dataset:

$$251 \quad \begin{cases} LAI = -2\ln(1 - f_{NDVI}) \\ f_{NDVI} = \frac{NDVI - NDVI_0}{NDVI_1 - NDVI_0} \end{cases} \quad (3)$$

252 where $NDVI_0 = 0.04$, $NDVI_1 = 0.52$

253 Evapotranspiration (ET) is then calculated as the ratio of GPP to WUE:

$$254 \quad ET = \frac{GPP}{WUE} \quad (4)$$

255 Under this framework, ET should be interpreted as an effective annual ecosystem-scale
256 evapotranspiration suitable for long-term WY attribution, rather than a detailed
257 partitioning of individual ET components. This modification allows the model to
258 estimate ET using dynamic WUE, replacing the static UWUE from the original model.
259 The dynamic nature of WUE enhances the model's ability to simulate ecosystem water
260 use across different environmental conditions and vegetation types.

261 Finally, the water yield (WY) is calculated as the difference between precipitation
262 (P) and ET:

$$263 \quad WY = P - ET \quad (5)$$

264 On an annual scale, WY is assumed to be approximately equal to runoff, as
265 changes in soil water storage over long periods (one year or longer) are considered
266 negligible (Xiao et al., 2020; Zhang et al., 2021b). Thus, the attribution of WY can also
267 be considered as the attribution of runoff. Accordingly, in this study WY is used as the
268 modelled output, while the term 'runoff' is reserved for observed streamflow or
269 literature values explicitly labelled as such. This approximation is most suitable for
270 annual to multi-year analyses in regions without substantial long-term groundwater
271 depletion or strong reservoir regulation.

272 **2.3 Attribution analysis framework**

273 To explore the combined and individual effects of climate, vegetation, and $[CO_2]$
274 change on water yield (WY), four scenarios were designed based on data from 1982 to
275 2017 (Table 2). Scenario 1 (Actual) aimed to validate the improved CCW model and
276 estimate the combined effects of climate, vegetation, and $[CO_2]$ change on WY by
277 allowing all variables to vary from 1982 to 2017. Scenario 2 (Vegetation Change)

278 focused on estimating the direct effects of vegetation change on WY by allowing
 279 vegetation variables (NDVI and LULC) to vary while keeping climate and [CO₂] fixed
 280 at 1982 levels. In this case, the trend in WY obtained reflects the impact of vegetation
 281 change alone. Scenario 3 (Climate Change) aimed to estimate the direct effects of
 282 climate change on WY by allowing climate variables (precipitation, temperature,
 283 relative humidity, solar radiation, and atmospheric pressure) to change, while fixing
 284 vegetation and [CO₂] at 1982 levels. This scenario helps isolate the effects of climate
 285 change on WY. Scenario 4 ([CO₂] Change) was designed to estimate the direct effects
 286 of [CO₂] change on WY by varying [CO₂] levels from 1982 to 2017, while climate and
 287 vegetation variables were fixed at 1982 levels. The resulting WY trend reflects the
 288 impact of [CO₂] change alone. The resulting WY series under each scenario represents
 289 the direct impact~~isolated impact~~ of the corresponding driver under the assumption that
 290 the other drivers are fixed.

291 **Table 2.** Scenario designs in the improved CCW model for WY attribution. LULC: Land use
 292 and land cover types; NDVI: Normalized difference vegetation index; TMP: Temperature;
 293 SRAD: Shortwave radiation; VPD: Vapor pressure deficit.

Scenarios	Vegetation		Climate					CO ₂	Purposes
	LULC	NDVI	P	T	RH	Srad	Pa	CO ₂	
S1 (baseline)	▲	▲	▲	▲	▲	▲	▲	▲	Validating the improved CCW model and estimating the combined effects of climate, vegetation, and CO ₂ change.
S2 (vegetation)	▲	▲	△	△	△	△	△	△	Estimating the direct effects of vegetation change.
S3 (climate)	△	△	▲	▲	▲	▲	▲	△	Estimating the direct effects of climate change.

S4
(CO₂)

△

△

△

△

△

△

△

▲

Estimating the
direct effects of
CO₂ change.

294 Note: The symbol “▲” denotes a changing input variable over time, whereas the symbol “△”
295 represents a fixed input variable at the level of the initial year (1982).

296 For each scenario, the long-term trend in annual WY over 1982–2017 was
297 quantified using the Theil–Sen estimator, yielding a robust slope. Here, “trend” refers
298 to the Theil–Sen slope of the annual WY series, representing the long-term monotonic
299 rate of change in WY over the study period. The relative contributions of climate,
300 vegetation, and [CO₂] to changes in WY were calculated using the following formula
301 (Ma et al., 2023; Wang et al., 2022):

$$302 \left\{ \begin{array}{l} RC_{vegetation} = \frac{trend_{vegetation}}{|trend_{vegetation}| + |trend_{climate}| + |trend_{CO_2}|} \times 100\% \\ RC_{climate} = \frac{trend_{climate}}{|trend_{vegetation}| + |trend_{climate}| + |trend_{CO_2}|} \times 100\% \\ RC_{CO_2} = \frac{trend_{CO_2}}{|trend_{vegetation}| + |trend_{climate}| + |trend_{CO_2}|} \times 100\% \end{array} \right. \quad (6)$$

303 where $trend_{vegetation}$, $trend_{climate}$, and $trend_{CO_2}$ denote the Theil–Sen slopes of
304 the annual WY series underrepresent the changes in water yield (WY) resulting from
305 vegetation, climate, and [CO₂] scenarios, respectively. These slopes represent the long-
306 term rates of WY change attributable to each driver within the scenario
307 frameworkchanges, respectively, as calculated in each scenario; the relative
308 contributions ($RC_{vegetation}$, $RC_{climate}$, and RC_{CO_2}) are expressed as percentages,
309 indicating the normalized magnitude of the scenario-derived direct effectsproportion of
310 each factor's influence on the overall changes in WY.

311 At each grid point, the absolute values of the relative contributions of each factor
312 (vegetation, climate, and [CO₂]) are compared. -For each grid point, we identify the
313 most significant contributor to water yield (WY) changes by comparing the relative
314 contributions of each factor. If the absolute values of the relative contributions of two
315 factors do not exceed 5%, then these two factors are considered joint significant

316 contributors to the changes in WY at that grid point (Jia et al., 2022). This approach
317 helps to highlight areas where the impacts of multiple factors are closely intertwined
318 and both play a critical role in influencing water yield, suggesting that their combined
319 effects are comparable in magnitude. In these cases, the relative contribution of each
320 factor is not significantly stronger than the other, indicating that their combined
321 influence on WY is equally important at the local scale.

322 The scenario analysis previously conducted revealed the relative contributions of
323 climate, vegetation, and [CO₂] to WY changes. However, these contributions arise from
324 both the intrinsic rate of change of each factor and the sensitivity of runoff to those
325 changes (the elasticity coefficient) (Yang and Yang, 2011). To gain a deeper
326 understanding of the changes in WY, we employ elasticity coefficients to quantify its
327 sensitivity to individual factor. We specifically focused on precipitation because,
328 despite not always having the highest sensitivity, it is integral to the hydrological cycle
329 and essential for assessing water yield (WY) under various climate change scenarios
330 (Liu et al., 2017). The elasticity of runoff refers to the variation in runoff depth resulting
331 from a 1% increase in each climatic variable (Xu et al., 2014). The absolute value of
332 elasticity reflects the sensitivity of runoff to various influencing factors. In other
333 methods, elasticity coefficients are typically calculated using an analytical expression
334 based on instantaneous changes in runoff corresponding to variations in a given factor
335 in a specific year (Fu et al., 2023; Liu et al., 2017; Yang and Yang, 2012). However, in
336 our study, we applied scenario-based analysis over the period of 1982 to 2017. This
337 extended temporal window allowed us to better account for the long-term effects and
338 interactions of multiple factors influencing WY. So we vary each factor (precipitation,
339 NDVI, and [CO₂]) by 1% relative to the baseline scenario S1 across the entire 1982-
340 2017 period. We then calculated the annual average runoff values from the adjusted
341 sequence and compared them with the average original baseline runoff values. The
342 difference between these two values, divided by the average baseline runoff value, gave
343 us the runoff change rate:

344
$$\frac{\Delta R_x}{R_x} = \frac{WY_{mean_x} - WY_{mean_x}}{WY_{mean_x}} \quad (7)$$

345 Mathematically, the elasticity coefficient is defined as the runoff change rate
 346 divided by 1%, and the formula is as follows:

347
$$\varepsilon_x = \frac{\frac{\Delta R_x}{R_x}}{\frac{\Delta x}{x}} = \frac{\frac{\Delta R_x}{R_x}}{1\%} \quad (8)$$

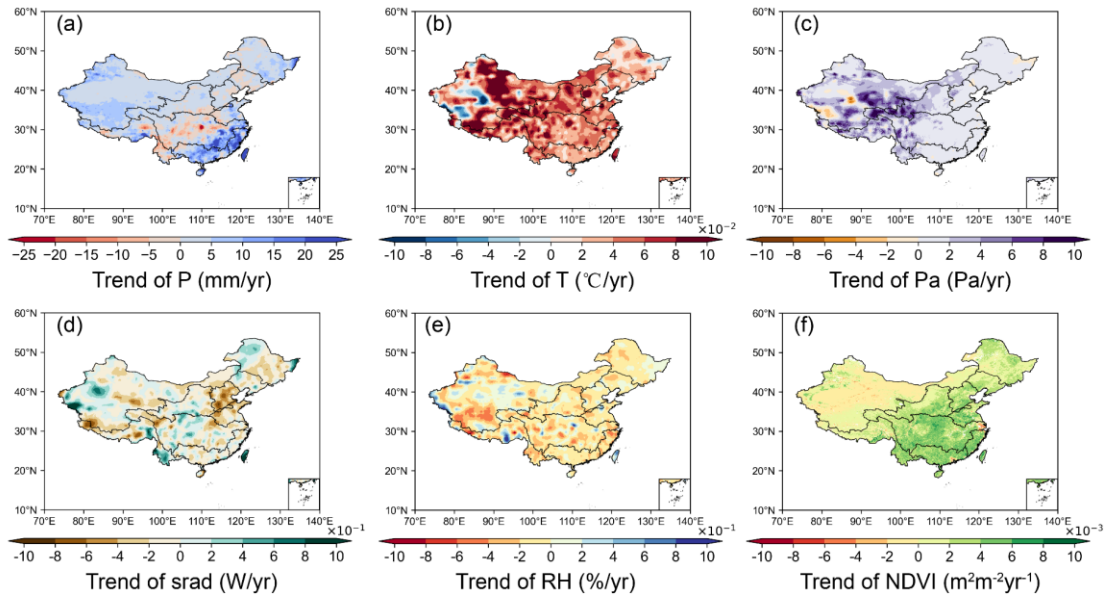
348 Generally, while the scenario analysis above has identified which factors are most
 349 influential based on their relative contributions, the elasticity coefficients allow us to
 350 explain why these factors are critical by demonstrating their respective impacts on WY
 351 through sensitivity analysis. This dual approach—combining both the changes in the
 352 factors and their elasticities—provides a more comprehensive understanding of the
 353 drivers behind the observed changes in WY, ensuring that the results of the scenario
 354 analysis are both meaningful and robust.

355 **3 Results**

356 **3.1 Changes in hydrometeorological variables**

357 Fig. 2 demonstrates the trends of annual precipitation, air temperature, relative
 358 humidity, atmospheric pressure, solar radiation, and NDVI across China during 1982-
 359 2017. Annual precipitation change exhibited a clear spatial distribution pattern,
 360 specifically decreases in central China, including the middle reaches of the Yellow
 361 River and the Yangtze River basins, and increases in the northwest and southeast. Air
 362 temperature exhibited a consistent warming trend across China. In contrast, relative
 363 humidity generally decreased across most China. Atmospheric pressure remained
 364 relatively stable. Regarding solar radiation, decreases were in northern China, while an
 365 increase was in southern regions. The decreasing solar radiation in northern China is
 366 likely due to increased aerosol concentrations (Liang et al., 2024). NDVI showed a
 367 significant increasing trend, which indicates an overall enhancement in vegetation

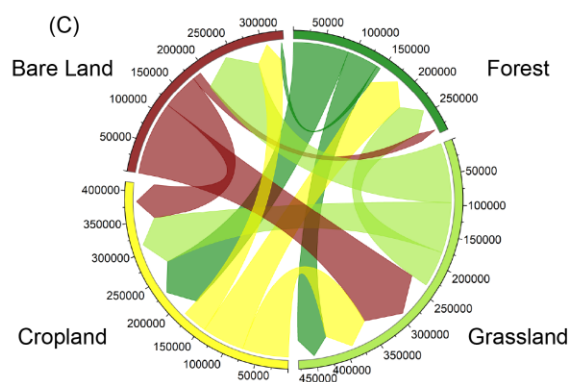
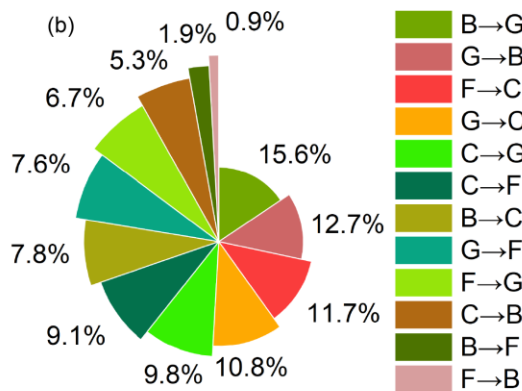
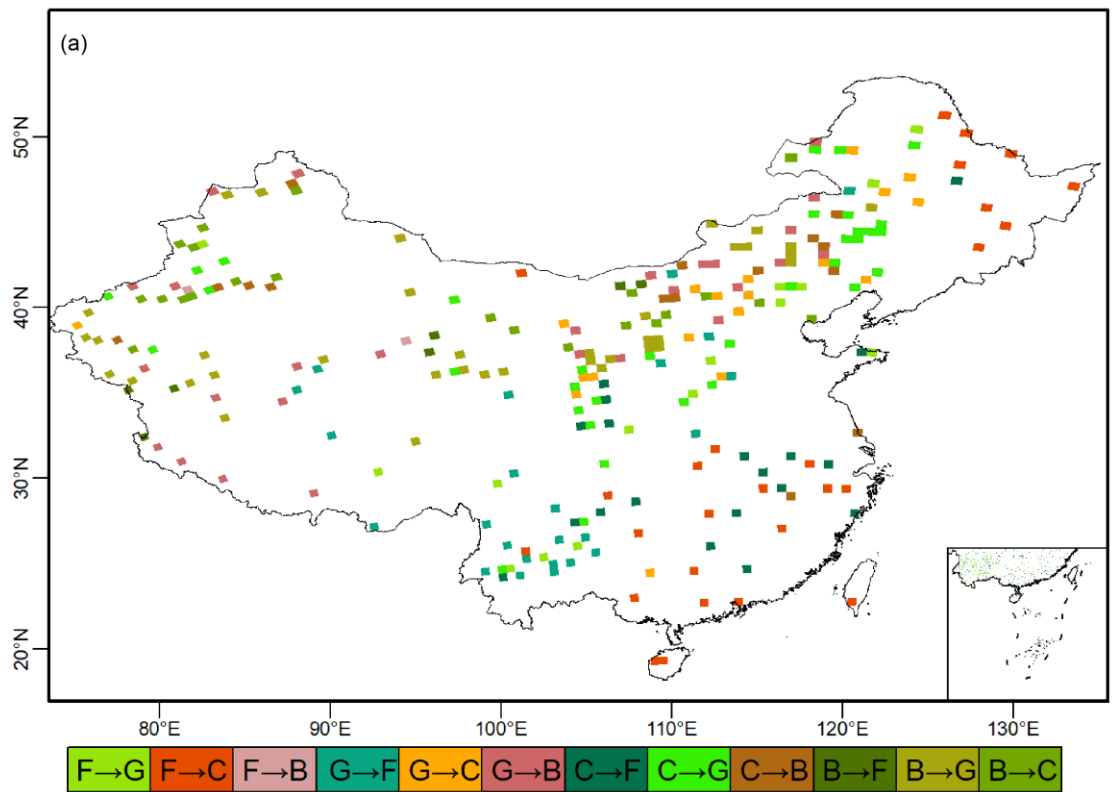
368 growth across China. This trend was especially prominent in central and eastern regions,
 369 including the Yellow River Basin and the Yangtze River Basin. In these regions, LULC
 370 changes, such as afforestation and agricultural practices, likely contributed to the
 371 observed increases in NDVI (Chen et al., 2019).



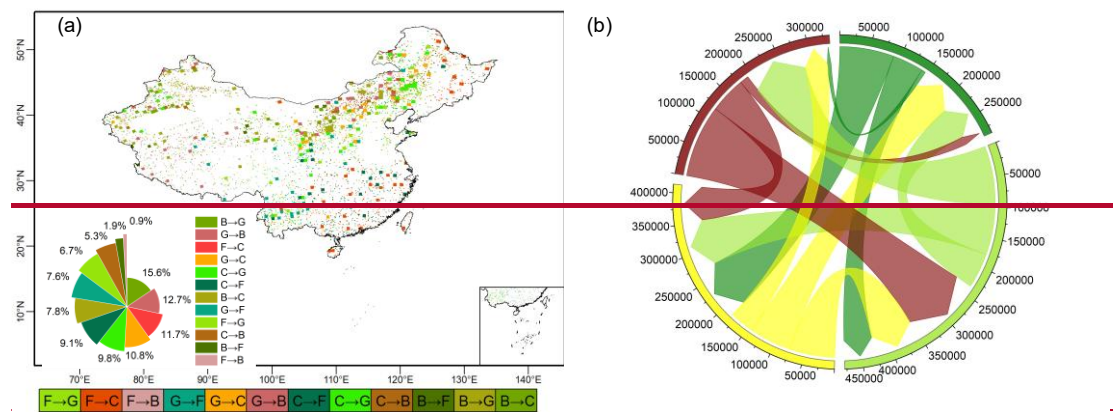
372
 373 **Figure 2.** Spatial patterns of trends in annual climatic and vegetation variables during 1982–
 374 2017. (a) precipitation (mm/yr); (b) air temperature ($^{\circ}\text{C}/\text{yr}$); (c) Atmospheric pressure (Pa/yr);
 375 (d) shortwave radiation ($\text{W}/\text{m}^2/\text{yr}$); (e) relative humidity ($\%/\text{yr}$); (f) NDVI (yr^{-1}).

376 Significant changes in land use and land cover (LULC) occurred in China during
 377 1982–2017, as illustrated in Fig. 3. Although the overall percentage distribution of
 378 major land cover types, namely grasslands, forests, croplands, and bare lands, remained
 379 relatively stable, these four categories dominated the landscape, with most changes
 380 concentrated within them. Notably, the transitions among these categories were
 381 characterized by mutual conversions, particularly from bare land to grasslands (Fig. 3).
 382 Spatially, the changes exhibited distinct regional patterns. In southern China, LULC
 383 changes were mainly characterized by the conversion of land to forests and grasslands.
 384 In contrast, the northeastern regions exhibited more complex transformations, with
 385 some areas shifting to bare land and croplands (Fig. 3).

386



387



388

389 **Figure 3.** Land use and land cover (LULC) changes from 1982 to 2017. (a) Spatial
 390 distribution of major conversion types among the four dominant LULC classes. F =

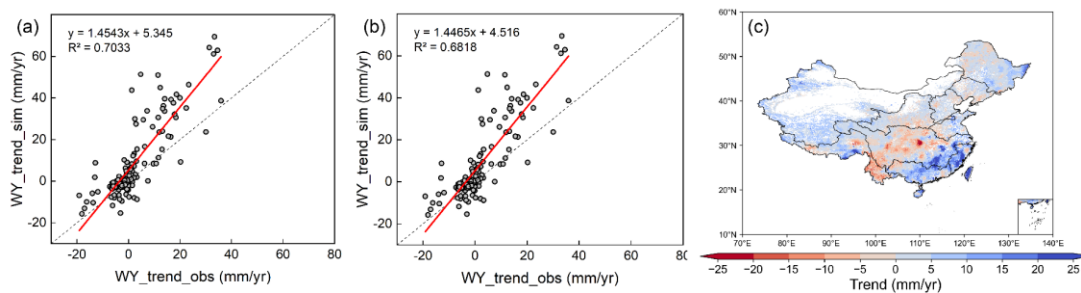
391 forest, G = grassland, C = cropland, and B = bare land. The arrow indicates the direction
 392 of conversion from the original land-cover type to the converted type. (b) Percentage
 393 share of each major conversion type in the total converted area (%). (c) Chord diagram
 394 of the corresponding conversion flows, where the labels around the circle denote land-
 395 cover classes, and the surrounding axis values indicate converted area (km²). (a) Spatial
 396 pattern distribution of LULC change; (b) Chord diagram of LULC conversion flows (unit: km²),
 397 where directional arrows represent transitions between land types (originating type → current
 398 type), with chord widths proportional to the converted areas. The figure illustrates the converted
 399 areas and does not include the unchanged regions.

400 3.2 Performance of the improved CCW model

401 As shown in Fig. 4a and b, the observed annual water yield (WY) and the
 402 simulated annual WY by the improved CCW model showed strong linear correlations
 403 ($R^2 = 0.7$), with the regression line slope being 1.45, R^2 being 0.7, and RMSE being
 404 9.54 ~~mm/year~~mm/yr. By contrast, the initial model without WUE showed weaker skill
 405 (slope = 1.45, $R^2 = 0.68$, RMSE = 9.62 ~~mm-yr⁻¹~~mm/yr), indicating that explicitly
 406 representing [CO₂]-induced regulation of water-use efficiency measurably improves
 407 accuracy and reduces bias.

408 The estimated annual WY trends had distinct spatial patterns (Fig. 4c), which
 409 closely aligned with that of precipitation. Specifically, decrease trends in WY occurred
 410 in the central regions of the Yellow River Basin and the middle section of the Yangtze
 411 River Basin, while increase trends were found in other regions, with the southeast
 412 exhibiting the highest rate of increase.

413

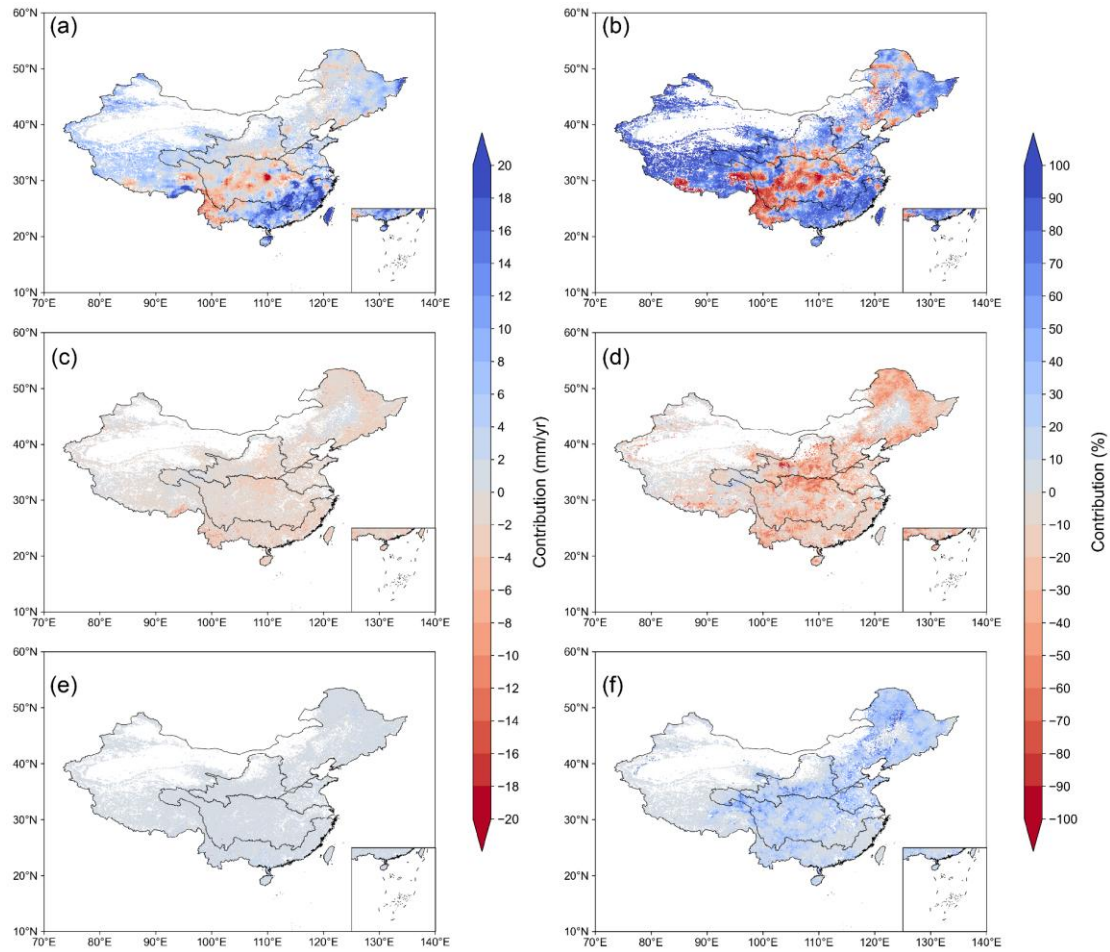


414

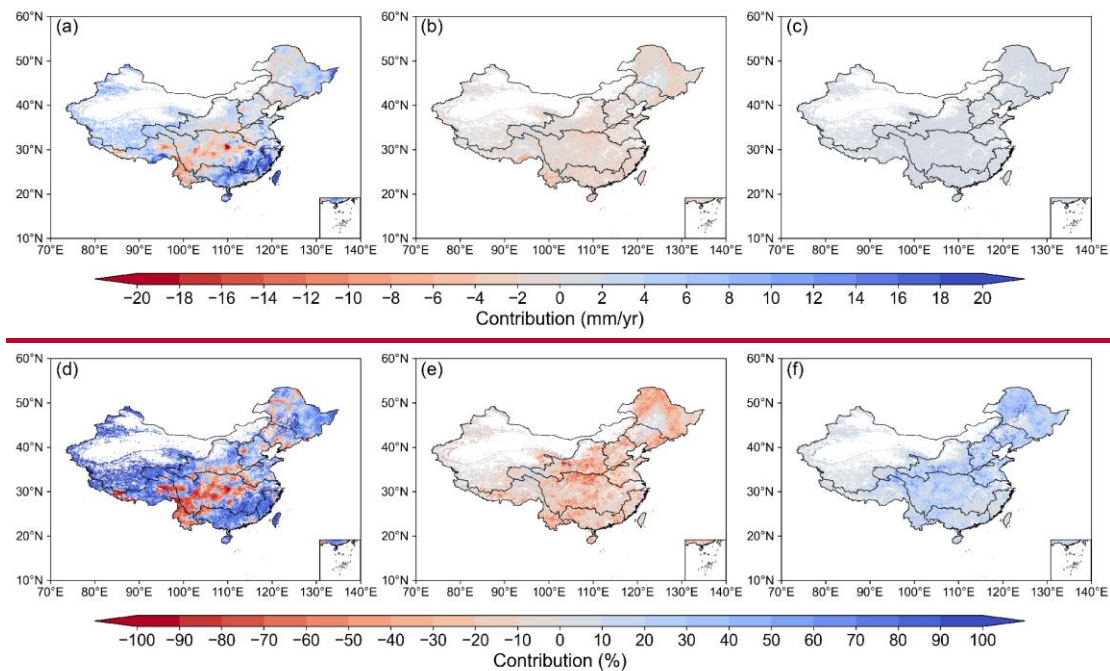
415 **Figure 4.** (a) Validation of simulated WY trend using the improved CCW model; (b) Validation
416 of simulated WY trend using the initial CCW model; (c) Spatial distribution of WY trends
417 under scenario S1(actual situation) during 1982–2017.

418 **3.3 Attribution analysis of annual WY changes**

419 Fig. 5 shows the distribution of WY changes caused by climate, vegetation, and
420 [CO₂] changes, integrating both absolute magnitude (Fig. 5a,c,-ed) and relative
421 dominance (Fig. ~~5d-fb,d,f~~) of their contributions. Climate-driven WY changes
422 exhibited marked spatial heterogeneity, with absolute increases exceeding 15 mm/yr in
423 southeastern China (Fig. 5a), corresponding to 60-90% relative contributions (Fig.
424 ~~5d5b~~). Central basins showed contrasting declines of 0-6 mm/yr under climate forcing,
425 while northeastern transitional zones displayed mixed positive/negative absolute
426 changes (Fig. 5a) despite maintaining 40-70% relative climate dominance (Fig. ~~5d5b~~).
427 This spatial heterogeneity aligned with precipitation change patterns (Fig. 2a).



428

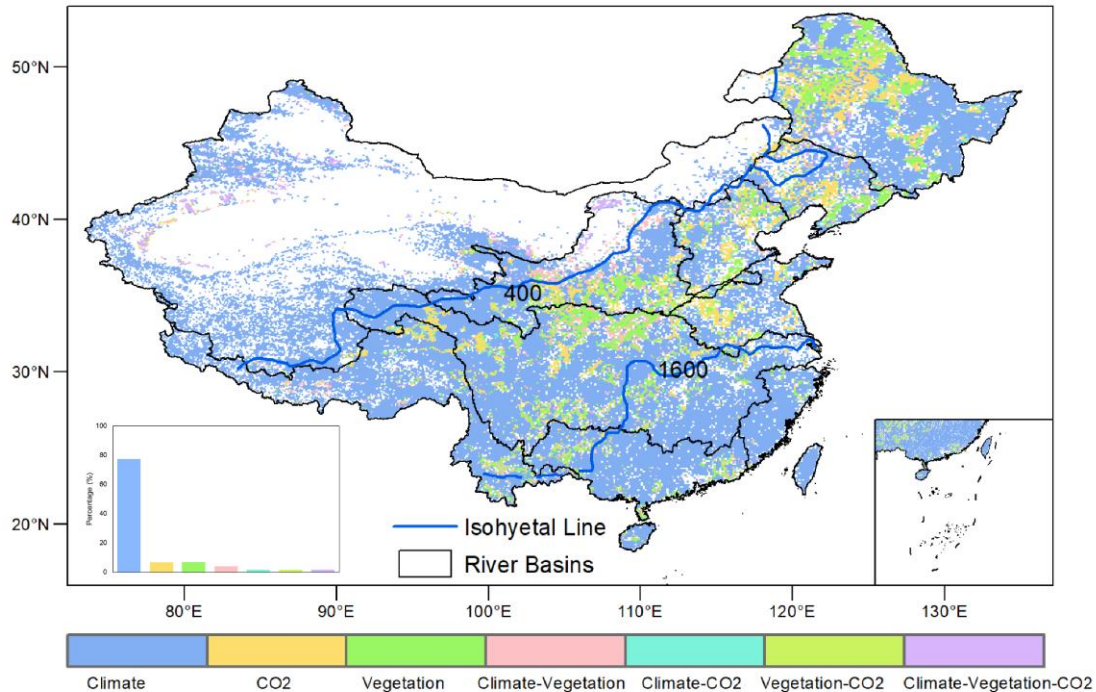


429

430 **Figure 5.** The absolute contributions of (a) climate, (bc) vegetation, and (ee) [CO₂], and the
 431 relative contributions of (db) climate, (ed) vegetation, and (f) [CO₂] to changes in WY trends
 432 for 1982-2017.

433 Vegetation-mediated WY reductions reached 0-6 mm/yr (Fig. 5b5c), accompanied
434 by 0-60% relative contributions (Fig. 5e5d). These effects originated from enhanced
435 evapotranspiration through land-use changes and NDVI-based greening, particularly
436 pronounced in central China. Specific regions in the Yangtze, Yellow, and northeastern
437 rivers showed vegetation-driven relative contributions reaching 40-60% (Fig. 5e5d).
438 [CO₂] effects generated limited direct absolute impacts (<5 mm/yr, Fig. 5e5e) but
439 exerted 10-40% relative influences (Fig. 5f) through stomatal closure mechanisms. This
440 process partially counteracted vegetation-related WY losses in transitional climates like
441 northeastern China, where competing drivers created complex ecohydrological
442 interactions (Fig. 5d-f).

443 Fig. 6 illustrated the spatial distribution of WY trend drivers over the past four
444 decades. Climate change was the dominant factor of WY variation in more than 70%
445 regions, mainly in the Northwest, Southwest, Southeast, Pearl River basins, and other
446 parts of the Yangtze and Yellow River basins. Vegetation changes ranked as the
447 secondary control, dominating WY changes in parts of the Yangtze, Yellow, Songhua,
448 Liao, and Hai Rivers. Remarkably, it was shown that the region where vegetation and
449 [CO₂] had the dominant influence mainly distributes within precipitation ranges of 400–
450 1600 mm. CO₂-induced effects were least influential at a national scale. This three-
451 tiered hierarchy—climate changes as the primary forcing, vegetation changes as the
452 secondary control, and [CO₂] effects as a localized modifier—reveals how hydrological
453 regimes govern the spatial succession of dominant drivers across China's diverse
454 ecohydrological gradients.

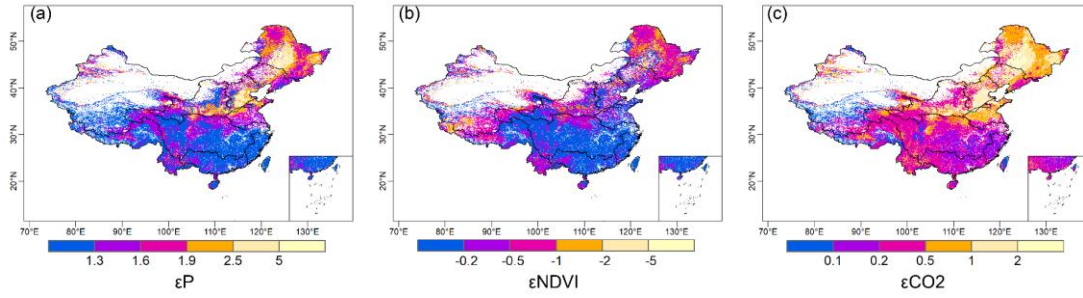


455

456 **Figure 6.** Spatial distributions of dominant factors controlling WY change. Driving factors
 457 include climate, vegetation, and [CO₂]. Climate: Areas where climate (e.g., precipitation,
 458 temperature) is the dominant factor influencing WY change; CO₂: Areas where [CO₂]
 459 is the primary driver of WY change; Vegetation: Areas where vegetation changes (e.g.,
 460 NDVI, LULC) primarily drive WY changes. Climate-Vegetation: Areas where both climate
 461 and vegetation jointly influence WY; Climate-CO₂: Areas where both climate and [CO₂]
 462 jointly contribute to WY change; Vegetation-CO₂: Areas where vegetation changes and [CO₂]
 463 jointly control WY; Climate-Vegetation-CO₂: Areas where the combined effect of climate,
 464 vegetation, and [CO₂] jointly controls WY change. Additionally, the approximate isohyetal line shown in
 465 the figure were derived based on annual precipitation data from 1982 to 2017.

466 **3.4 Elasticity of WY to main variables**

467 The sensitivity of WY to precipitation (ϵ_P), NDVI (ϵ_{NDVI}), and [CO₂] (ϵ_{CO_2})
 468 exhibits distinct spatial patterns in (Fig. 7). Nationally averaged elasticity coefficients
 469 showed that a 10% increase in precipitation, [CO₂], and NDVI altered WY by 15.5%
 470 ($\epsilon_P=1.55$), 5.5% ($\epsilon_{CO_2}=0.55$), and -4.4% ($\epsilon_{NDVI}=-0.44$), respectively, indicating that,
 471 in terms of the sensitivity of runoff to changes in each factor, the ranking was
 472 precipitation > [CO₂] > NDVI.



473

474 **Figure 7.** Spatial distribution of elasticity coefficients of WY relative to changes in
 475 hydrological variables such as (a) annual precipitation, (b) NDVI, and (c) [CO₂].

476 The elasticity coefficients of precipitation (ϵP), [CO₂] (ϵCO_2), and vegetation
 477 ($|\epsilon NDVI|$) all exhibited a coherent latitudinal decline across China's river basins,
 478 showing systematically higher sensitivity in northern regions than southern
 479 counterparts. Quantitatively, ϵP decreased from 2.09 in the Songhua River basin to 1.15
 480 in the Southeastern Basin, accompanied by similar reductions in $|\epsilon NDVI|$ (from 0.76 to
 481 0.13) and ϵCO_2 (from 1.08 to 0.16) (Table 3).

482 A distinct abrupt transition zone in elasticity coefficients was identified around
 483 33°N, closely aligning with China's traditional North-South physiographic divide.
 484 Around the zone, elasticity coefficients exhibited an abrupt decline from the Yellow
 485 River Basin to the Yangtze River Basin. Specifically, the Yellow River Basin showed
 486 higher sensitivities to precipitation ($\epsilon P=1.87$), [CO₂] ($\epsilon CO_2=0.86$), and NDVI
 487 ($\epsilon NDVI=-0.53$), which were approximately 1.4, 2.8, and 2.8 times greater, respectively,
 488 than those in the Yangtze River Basin ($\epsilon P=1.31$, $\epsilon CO_2=0.31$, $\epsilon NDVI=-0.19$).

489 **Table 3.** Elasticity Coefficients of Runoff to Precipitation, NDVI, and CO₂ in Different
 490 Watersheds

Dataset	ϵP	$\epsilon NDVI$	ϵCO_2
Songhua River basin	2.09	-0.76	1.08
Hai River basin	2.13	-0.44	1.12
Yellow River basin	1.87	-0.53	0.86
Yangtze River Basin	1.31	-0.19	0.31
Huai River basin	1.64	-0.18	0.63
Pearl River basin	1.25	-0.17	0.25
Southeast Rivers	1.15	-0.13	0.15

491 Note: Some LULC types were excluded from the analysis. Due to many missing data points,
492 the Liao River, Southwest, and Northwest river basins were also omitted.

493 **4 Discussion**

494 **4.1 Strength of the attribution analysis framework**

495 To address limitations in current methods for analysing the effects of climate,
496 vegetation, and [CO₂] on runoff changes, we developed an attribution analysis
497 framework based on the improved CCW model. This framework has been improved in
498 three aspects. Firstly, the explicit and mechanistic integration of vegetation dynamics
499 and [CO₂] effects overcomes the oversimplifications inherent in conventional
500 approaches. Traditional Budyko-based frameworks often attribute vegetation effects to
501 temporal variations in the Budyko parameter (n)parameter "n" by either statistically
502 regressing the Budyko parameter "n" against vegetation proxies such as NDVI (Liu et
503 al., 2024; Tan et al., 2023) or simplistically equating the Budyko parameter "n" to
504 vegetation effects (Li et al., 2020b; Zhou et al., 2023). Such approaches conflate
505 structural vegetation changes (e.g., leaf area index) with physiological adjustments (e.g.,
506 CO₂-induced stomatal closure), thereby obscuring the independent roles of vegetation
507 dynamics and [CO₂]. For example, while rising [CO₂] levels directly reduce stomatal
508 conductance and transpiration, Budyko-based studies often misinterpret this effect as
509 part of the the Budyko "n" parameter's variability, erroneously attributing it to
510 vegetation changes (Zeng et al., 2020). In contrast, our framework mechanistically
511 separates these pathways by explicitly describing the stomatal conductance–WUE
512 relationship based on plant physiological theory. Elevated [CO₂] reduces stomatal
513 aperture, thereby lowering stomatal conductance and transpiration flux while only
514 modestly increasing carbon assimilation, leading to an overall enhancement in water-
515 use efficiency (WUE). This process is represented by the Medlyn-type stomatal
516 conductance model (Medlyn et al., 2011), which links photosynthetic rate (A),
517 transpiration (T), and vapor pressure deficit (D) as:

518
$$\frac{A}{T} = \frac{C_a P_a}{1.6(D + g_1 \sqrt{D})}$$

519 where C_a is atmospheric CO₂ concentration, P_a is air pressure, D is vapor pressure
520 deficit, and g_1 is an empirical slope parameter that quantifies plant sensitivity to CO₂
521 and humidity. According to this formulation, rising [CO₂] increases while reducing
522 stomatal conductance, which in turn suppresses transpiration more strongly than
523 photosynthesis, resulting in higher WUE. This mechanistic representation enables our
524 framework to capture the direct physiological CO₂ effect on evapotranspiration, which
525 is otherwise masked in Budyko-type models where CO₂ impacts are embedded
526 implicitly in PET or the “n” parameter.

527 Secondly, unlike Budyko-based methods that indirectly represent [CO₂] impacts
528 through adjustments to potential evapotranspiration (PET)—a practice conflating [CO₂]
529 effects with meteorological drivers like radiation and wind—our framework explicitly
530 quantifies CO₂'s physiological influence on actual evapotranspiration (AET) by
531 mechanistically modeling its role in stomatal conductance and water-use efficiency
532 (WUE). Elevated [CO₂] reduces stomatal conductance and transpiration while
533 moderately enhancing carbon assimilation, partially offsetting water losses associated
534 with vegetation greening. For example, our results show that reduction in transpiration
535 due to CO₂-driven stomatal closure offsets water losses, a mechanism entirely masked
536 in Budyko frameworks where [CO₂] effects are ambiguously embedded in PET
537 adjustments or erroneously attributed to vegetation structural changes via the “n”
538 parameter (Liu et al., 2024). This coupled regulation clarified how water and energy
539 jointly constrain evapotranspiration, particularly in 400-1600 mm precipitation zones.
540 In these regions, vegetation growth enhanced transpiration and root water uptake until
541 increasing atmospheric aridity imposed physiological constraints, while rising [CO₂]
542 partially counteracted this effect by improving water-use efficiency through stomatal
543 closure. As a result, the framework provided a more mechanistically grounded

544 understanding of how [CO₂] ~~fertilization~~—modulates ecosystem water use and
545 hydrological responses at regional scales.

546 Compared with the original CCW model using static UWUE, the improved
547 framework does not merely provide a modest statistical improvement. Its main advance
548 is that it allows WUE to vary dynamically with [CO₂], VPD, and canopy structure,
549 thereby explicitly representing the physiological regulation of ET by rising [CO₂]. This
550 makes it possible to distinguish LAI (vegetation structural) water consumption from
551 [CO₂]-induced stomatal water-saving effects, which is essential for interpreting why
552 WY responses differ across regions and why [CO₂] can partly offset vegetation-related
553 WY reductions.

554 Thirdly, while numerous studies have conducted runoff attribution analysis at the
555 basin scale (Liu et al., 2024, 2017; Yang et al., 2022), our grid-scale approach
556 transcends the spatial constraints of fixed watershed boundaries by resolving regional
557 heterogeneity in hydrological drivers. Conventional basin-aggregated methods obscure
558 critical intra-basin differences—for instance, our analysis reveals that grids in the upper
559 Yangtze River basin, where precipitation change dominates runoff trends, necessitate
560 climate scenario-based water resource planning. In contrast, mid-basin grids with
561 significant NDVI-driven greening exhibit pronounced WY reductions, highlighting the
562 need for vegetation management strategies that restrict excessive afforestation in water-
563 sensitive areas (Sun et al., 2022; Yang et al., 2021). By decoupling analysis from rigid
564 watershed boundaries, our framework enables targeted strategies such as restricting
565 reforestation in water-stressed grids or selecting CO₂-adapted vegetation species,
566 thereby aligning management actions with localized climate-vegetation-hydrology
567 interactions.

568 **4.2 New insights into attribution analysis**

569 Our findings highlighted climate change as the dominant driver of water yield (WY)
570 changes (contributing >70%), consistent with other assessments (Table 4), yet reveal

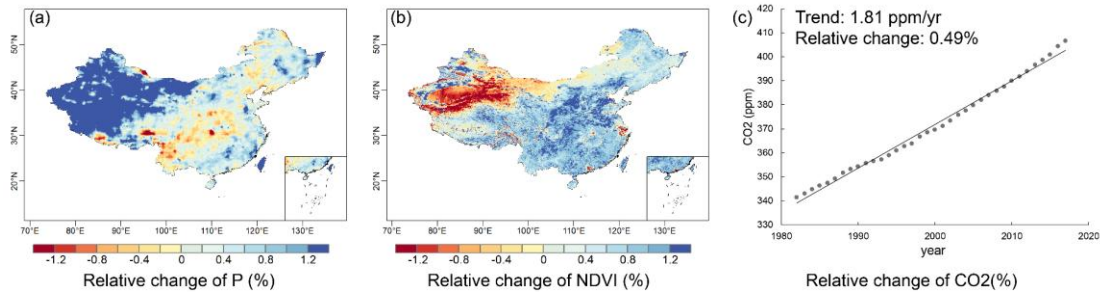
571 critical regional divergences. Climate impacts dominated in the Northwest and
572 Southwest River Basins, as well as parts of the Yangtze, Yellow, Southeast, and Pearl
573 River Basins, while vegetation and [CO₂] effects prevailed in central China (parts of
574 the Yangtze, Yellow, Songhua, Liao, and Hai River basin)—a spatial pattern slightly
575 distinct from earlier studies. Although previous studies identified human activities as
576 the primary driver in some northern basins (Liao, Hai, and Yellow River Basins) ((Yang
577 et al., 2022), their long-term study (1965-2018) diluted the gradually strengthening
578 vegetation signals after 2000 mentioned in other studies (Liu et al., 2017; Sun et al.,
579 2023) through time-averaging. Our findings now confirm the emerging importance of
580 vegetation dynamics in southern basins like the Yangtze through our symmetric 1982-
581 2017 study period. This basin-scale contrast is also consistent with a broader
582 hydroclimatic gradient, as vegetation and [CO₂] effects become relatively more
583 important in the intermediate 400–1600 mm precipitation zone. Although the
584 improvement in overall model performance is modest, the main value of introducing
585 dynamic WUE is not limited to statistical enhancement. More importantly, this
586 refinement allows the improved CCW model to explicitly represent the physiological
587 effect of rising [CO₂] on evapotranspiration, which cannot be resolved by the original
588 static-UWUE formulation. As a result, the model can distinguish vegetation-driven
589 increases in water consumption from [CO₂]-induced stomatal water-saving effects,
590 thereby providing new insight into why WY responses differ across regions and why
591 [CO₂] can partially offset vegetation-related WY reductions, especially in transitional
592 hydroclimatic zones.

593 **Table 4.** Comparative studies of the contribution of climate variability and vegetation to runoff
594 changes.

Reference	Study region	Study period	Method/Model	Driving factors
(Wei et al., 2024)	Global	1981-2020	Trendy phase 11 +ROF	Climate change
(Liu et al., 2024)	Global	1984-2010; 2000-2100	Improved Budyko	Precipitation

(Zhou et al., 2023)	Global	1850-2014; 2015-2100	Improved Budyko + CMIP6	Land surface changes
(Tan et al., 2023)	Global	2003-2016; 1982-2016	Improved Budyko	Effective precipitation
(Yang et al., 2022)	China	1965-2018	Budyko	P: Northwest river basin, Southwest river basin, Yangtze river basin, Southeast river basin, and Pearl river basin; <u>Budyko parameter (n)</u> : Liaohe river basin, Haihe river basin, Yellow river Basin, Songhuajiang river basin, and Huaihe river basin
(Zhang et al., 2022b)	Yangtze River	2001-2018	CCW Model	Climate variability
(Chen et al., 2022)	Six river basins in China	1982-2015	Gray Relational Analysis (GRA)	Precipitation
(Zhai and Tao, 2021)	China	1982-2015	VIC Model	Climate change
(Li et al., 2020a)	Yihe River	1960-2013	SWAT+WRF	Climate variability
(Shen et al., 2017)	China	1960-2010	Budyko	Underlying surface change (n): the Songhua Basin, the Liaohe Basin and the Haihe Basin; Climate change: in other basins.

595 Elasticity analysis (Section 3.4) revealed distinct sensitivities of WY to
596 environmental drivers: precipitation exhibited the highest elasticity coefficient for the
597 whole China ($\epsilon_P = 1.55$), followed by CO_2 ($\epsilon_{CO_2} = 0.55$) and NDVI ($\epsilon_{NDVI} = -0.44$).
598 However, spatial analysis showed that vegetation and $[CO_2]$ collectively dominated
599 WY changes in 400–1600 mm/yr precipitation zones, despite their lower sensitivity
600 rankings. The joint effect of elasticity and the magnitude of driver change ~~that~~
601 determines each driver’s net contribution. In the 400–1600 mm/yr precipitation zones,
602 NDVI displayed (Fig. 8) a larger relative temporal variation compared with
603 precipitation, which fluctuated within a narrower range. Consequently, vegetation’s
604 stronger relative change amplified its hydrological influence, overriding its lower
605 elasticity. Similarly, CO_2 ’s historical impact was constrained by its slow accumulation
606 rate (0.49%/yr), yet its relatively high elasticity positions it as a latent driver.
607



608

609 **Figure 8.** Spatial distribution of relative changes of different variables: (a) annual precipitation,
 610 and (b) NDVI.

611 This historical constraint, however, belied CO₂'s transformative potential under
 612 intensified forcing scenarios. CMIP6 SSP585 projections indicate [CO₂] will rise at
 613 2.34%/yr—nearly fivefold faster than historical rates (Cheng et al., 2022). Using the
 614 historical elasticity coefficient as a simple sensitivity-based approximation~~At this~~
 615 ~~trajectory~~, CO₂'s elasticity would drive a +1.29% annual WY increase, eclipsing both
 616 vegetation greening effects and even surpassing precipitation-driven changes in some
 617 regions. However, this estimate assumes that the historical [CO₂] elasticity remains
 618 unchanged and does not account for possible counteracting effects such as rising VPD,
 619 drought stress, or saturation of WUE under elevated [CO₂] (Adams et al., 2020; Li et
 620 al., 2023). Nevertheless, the result suggests that [CO₂] may become a more important
 621 hydrological modifier under strong future forcing, particularly in the 400–1600 mm
 622 precipitation zones.~~Such reversal underscores the imperative to prioritize [CO₂] in~~
 623 ~~long-term water management, particularly in 400–1600 mm/yr precipitation zones.~~

624 From a policy perspective, these spatial contrasts have distinct implications for
 625 regional water management. In vegetation-dominated regions such as the Yangtze and
 626 Huang river basins, enhancing ecosystem-based restoration, optimizing vegetation
 627 composition, and preventing overgreening that may suppress runoff should be
 628 prioritized. Conversely, in climate-dominated areas such as Northwest and Southeast
 629 China, adaptive measures emphasizing precipitation variability, water storage capacity,
 630 and drought resilience are crucial. Recognizing and tailoring water management

631 strategies to these driver-specific regimes can enhance the effectiveness of both
632 ecological restoration and climate adaptation programs across China.

633 **4.3 Uncertainty in attribution analysis**

634 This study provides valuable insights into the relationship between water resources
635 management and environmental changes, which can guide environmental management
636 strategies. However, several limitations exist that need to be addressed in future work
637 to improve the accuracy and robustness of the results.

638 Firstly, ~~the improved CCW model does not account for the variation and specific~~
639 ~~values of f_i , assuming f_i is 0. the adopted WUE formulation is defined at the ecosystem~~
640 ~~scale, but the present implementation simplifies the interception term by assuming $f_i =$~~
641 ~~0. Soil evaporation is still implicitly represented through the LAI-based partitioning~~
642 ~~term, whereas canopy interception is not explicitly allowed to vary across space or time.~~
643 ~~This simplification may bias the absolute magnitude of ET and WY, particularly in~~
644 ~~humid and forested regions, although its influence on long-term WY trends is expected~~
645 ~~to be smaller than on short-term hydrological fluxes. In reality, f_i represents the ratio of~~
646 ~~interception evaporation to total evaporation, and in regions with abundant vegetation,~~
647 ~~f_i is not zero.~~ Despite this, considering the small change of f_i in the current year (Zhao
648 et al., 2022), its influence on runoff trends is negligible in our study (Cheng et al., 2017).
649 However, future work should prioritize its calculation to improve the precision of WY
650 estimates.

651 Secondly, the complex interrelationships among climate, vegetation, and [CO₂]
652 cannot be fully disentangled. Vegetation exhibits tight biophysical interactions and
653 feedback with climate, making it difficult to separate the impacts of climate change,
654 vegetation dynamics, and [CO₂] on hydrological responses in a strictly independent
655 manner. Changes in vegetation, such as NDVI, reflect a combination of climate change,
656 human activities (e.g., reforestation and irrigation), and natural vegetation growth.
657 Additionally, vegetation greening in upwind regions can increase atmospheric moisture,

658 potentially enhancing precipitation downwind (Zhang et al., 2021a), which may
659 counteract some of the negative impacts of increased evapotranspiration on local WY.
660 Although the climate data used in our model may implicitly capture some of these
661 feedbacks, they cannot be explicitly separated in this analysis. Consequently, our results
662 represent an attempt to estimate the direct first-order net impacts of climate, vegetation
663 greening, and [CO₂] increase on WY ~~Consequently, our results represent an attempt to~~
664 ~~estimate the direct first-order net impacts of climate, vegetation greening, and [CO₂]~~
665 ~~increase on WY~~ (Zhang et al., 2021b). Future research should adopt more
666 comprehensive models that consider soil-vegetation-atmosphere interactions to better
667 differentiate the contributions of each driving factor to WY ~~better differentiate the~~
668 ~~contributions of each driving factor to WY.~~

669 Thirdly, the improved CCW model does not incorporate certain human activities,
670 such as large-scale irrigation, groundwater pumping, and reservoir regulation, which
671 also limits the assumption of $WY = P - ET$ with negligible storage change. This
672 assumption is mainly appropriate at the annual scale and becomes less reliable in
673 regions where long-term groundwater depletion or reservoir operation substantially
674 alters water storage and runoff routing. ~~which should be incorporated in future studies.~~
675 For instance, irrigation can sustain vegetation greening during dry seasons, potentially
676 amplifying the vegetation–climate feedback on water yield. ~~–~~Incorporating such
677 anthropogenic processes into the CCW framework through coupled irrigation and water
678 management modules would enable more comprehensive attribution analyses in future
679 studies. Our research also excludes water bodies and built-up land. While urbanization
680 can increase flood risks due to the growing proportion of impervious surfaces (Wasko
681 and Sharma, 2017), these land-use changes represent a small portion of China’s land
682 area.

683
684 Finally, the future impact of vegetation greening on hydrological dynamics will
685 depend on projected climate warming and drying trends, the persistence of vegetation

686 greening, [CO₂] changes, and the complex feedbacks between climate, soil, and
687 vegetation. In particular, the simple elasticity-based SSP585 estimate of the [CO₂]
688 effect does not account for concurrent changes in VPD or possible saturation of WUE
689 under elevated [CO₂] and drought stress, which adds uncertainty to the future WY
690 response. These interactions require long-term study, and future research will involve
691 more extensive monitoring to better capture these evolving dynamics.

692 **5 Conclusions**

693 In this study, we improved the CCW model incorporating dynamic water use
694 efficiency (WUE) calculation to explicitly represent CO₂-physiological feedback on
695 water yield. This mechanistic improvement enabled comprehensive national-scale
696 assessment quantifying the relative contributions of climate forcing, vegetation
697 structural changes, and CO₂-driven stomatal regulation to water yield (WY) dynamics
698 in China. The main conclusions are as follows:

699 The improved CCW model effectively simulated WY variations in most basins
700 under increased [CO₂] scenarios, demonstrating its applicability and reliability in
701 modeling WY changes.

702 Climate change, particularly variations in precipitation, emerged as the primary
703 driver influencing WY, displaying significant regional disparities in its effects.
704 Vegetation changes constituted the second most critical factor, predominantly resulting
705 in WY reduction, notably in central China. While the effect of CO₂-induced stomatal
706 closure on WY was comparatively minor. Spatial analysis aligned with isohyetal lines
707 further revealed that vegetation change and [CO₂] exerted greater influence within the
708 400–1600 mm precipitation range.

709 The elasticity analysis of WY indicated that northern basins exhibit higher
710 sensitivity to influencing factors, whereas southern basins demonstrate relatively lower
711 elasticity. Specifically, the absolute elasticity coefficients for the whole China were
712 ranked in descending order as follows: precipitation > [CO₂] > NDVI. Thus,

713 accelerating [CO₂] rise (2.34% /yr under SSP585) will amplify its hydrological role,
714 potentially elevating CO₂-driven WY increases to +1.29% annually by 2100, surpassing
715 climate and vegetation impacts, although this estimate does not account for concurrent
716 VPD changes or possible WUE saturation.

717 These insights provide a nuanced understanding of regional hydrological
718 responses, essential for sustainable water resource management under changing
719 environmental conditions.

720 **Acknowledgements**

721 This research was supported by the China National Key R&D Program (grant no.
722 2024YFF1306901)- and Open Research Fund Program of the State Key Laboratory of
723 Hydroscience and Engineering (grant no. sklhse-KF-2026-A-03).

724 **Data Availability Statement**

725 Datasets used for driving models were obtained from different sources described
726 in Table 1. All the data related to our results in this study can be found online: the NDVI
727 data (<https://doi.org/10.6084/m9.figshare.c.7002225.v1>); the climate data
728 (<https://www.tpdc.ac.cn/zh-hans/data/8028b944-daaa-4511-8769-965612652c49/>); the
729 land use and land cover (LULC) data (<https://zenodo.org/records/8239305>) (Liu et al.,
730 2023); and the [CO₂] (<http://cdiac.esd.ornl.gov/ftp/trends/co2/maunaloa.co2>), except
731 for the streamflow records for hydrological gauging stations, which are available upon
732 reasonable request.

733 **Author contributions**

734 HS designed the study, developed the model code, did the simulation experiments,
735 and wrote the first draft of the paper. HY designed the research and edited the
736 manuscript. CL provided feedback on the results and edited the manuscript.

737 **Competing interests**

738 The contact author has declared that neither they nor their co-authors have any
739 competing interests.
740

741 **Reference**

- 742 Adams, M. A., Buckley, T. N., and Turnbull, T. L.: Diminishing CO₂-driven gains in
743 water-use efficiency of global forests, *Nat. Clim. Chang.*, 10, 466–471,
744 <https://doi.org/10.1038/s41558-020-0747-7>, 2020.
- 745 Chen, C., Park, T., Wang, X., Piao, S., Xu, B., Chaturvedi, R. K., Fuchs, R., Brovkin,
746 V., Ciais, P., Fensholt, R., Tømmervik, H., Bala, G., Zhu, Z., Nemani, R. R., and
747 Myneni, R. B.: China and India lead in greening of the world through land-use
748 management, *Nat Sustain*, 2, 122–129, <https://doi.org/10.1038/s41893-019-0220-7>,
749 2019.
- 750 Chen, S., Fu, Y. H., Geng, X., Hao, Z., Tang, J., Zhang, X., Xu, Z., and Hao, F.:
751 Influences of Shifted Vegetation Phenology on Runoff Across a Hydroclimatic
752 Gradient, *Front. Plant Sci.*, 12, 802664, <https://doi.org/10.3389/fpls.2021.802664>, 2022.
- 753 Cheng, L., Zhang, L., Wang, Y.-P., Canadell, J. G., Chiew, F. H. S., Beringer, J., Li, L.,
754 Miralles, D. G., Piao, S., and Zhang, Y.: Recent increases in terrestrial carbon uptake
755 at little cost to the water cycle, *Nat Commun*, 8, 110, <https://doi.org/10.1038/s41467-017-00114-5>, 2017.
- 757 Cheng, W., Dan, L., Deng, X., Feng, J., Wang, Y., Peng, J., Tian, J., Qi, W., Liu, Z.,
758 Zheng, X., Zhou, D., Jiang, S., Zhao, H., and Wang, X.: Global monthly gridded
759 atmospheric carbon dioxide concentrations under the historical and future scenarios,
760 *Sci Data*, 9, 83, <https://doi.org/10.1038/s41597-022-01196-7>, 2022.
- 761 Fu, J., Liu, B., Wang, W., and Fei, E. X.: Evaluating main drivers of runoff changes
762 across China from 1956 to 2000 by using different budyko-based elasticity methods,
763 *Journal of Environmental Management*, 329, 117070,
764 <https://doi.org/10.1016/j.jenvman.2022.117070>, 2023.
- 765 Gan, G., Liu, Y., and Sun, G.: Understanding interactions among climate, water, and
766 vegetation with the Budyko framework, *Earth-Science Reviews*, 212, 103451,
767 <https://doi.org/10.1016/j.earscirev.2020.103451>, 2021.
- 768 Gutman, G. and Ignatov, A.: The derivation of the green vegetation fraction from
769 NOAA/AVHRR data for use in numerical weather prediction models, *International*
770 *Journal of Remote Sensing*, 19, 1533–1543, <https://doi.org/10.1080/014311698215333>,
771 1998.
- 772 He, J., Yang, K., Tang, W., Lu, H., Qin, J., Chen, Y., and Li, X.: The first high-
773 resolution meteorological forcing dataset for land process studies over China, *Sci Data*,
774 7, 25, <https://doi.org/10.1038/s41597-020-0369-y>, 2020.

775 Howell, T. A. and Dusek, D. A.: Comparison of Vapor-Pressure-Deficit Calculation
776 Methods—Southern High Plains, *J. Irrig. Drain Eng.*, 121, 191–198,
777 [https://doi.org/10.1061/\(ASCE\)0733-9437\(1995\)121:2\(191\)](https://doi.org/10.1061/(ASCE)0733-9437(1995)121:2(191)), 1995.

778 Jia, Y., Li, C., Yang, H., Yang, W., and Liu, Z.: Assessments of three
779 evapotranspiration products over China using extended triple collocation and water
780 balance methods, *Journal of Hydrology*, 614, 128594,
781 <https://doi.org/10.1016/j.jhydrol.2022.128594>, 2022.

782 Jiao, Y., Lei, H., Yang, D., Huang, M., Liu, D., and Yuan, X.: Impact of vegetation
783 dynamics on hydrological processes in a semi-arid basin by using a land surface-
784 hydrology coupled model, *Journal of Hydrology*, 551, 116–131,
785 <https://doi.org/10.1016/j.jhydrol.2017.05.060>, 2017.

786 Lammertsma, E. I., Boer, H. J. D., Dekker, S. C., Dilcher, D. L., Lotter, A. F., and
787 Wagner-Cremer, F.: Global CO₂ rise leads to reduced maximum stomatal conductance
788 in Florida vegetation, *Proc. Natl. Acad. Sci. U.S.A.*, 108, 4035–4040,
789 <https://doi.org/10.1073/pnas.1100371108>, 2011.

790 Li, B., Shi, X., Lian, L., Chen, Y., Chen, Z., and Sun, X.: Quantifying the effects of
791 climate variability, direct and indirect land use change, and human activities on runoff,
792 *Journal of Hydrology*, 584, 124684, <https://doi.org/10.1016/j.jhydrol.2020.124684>,
793 2020a.

794 Li, F., Xiao, J., Chen, J., Ballantyne, A., Jin, K., Li, B., Abraha, M., and John, R.: Global
795 water use efficiency saturation due to increased vapor pressure deficit, *Science*, 381,
796 672–677, <https://doi.org/10.1126/science.adf5041>, 2023.

797 Li, H., Shi, C., Zhang, Y., Ning, T., Sun, P., Liu, X., Ma, X., Liu, W., and Collins, A.
798 L.: Using the Budyko hypothesis for detecting and attributing changes in runoff to
799 climate and vegetation change in the soft sandstone area of the middle Yellow River
800 basin, China, *Science of The Total Environment*, 703, 135588,
801 <https://doi.org/10.1016/j.scitotenv.2019.135588>, 2020b.

802 Li, H., Cao, Y., Xiao, J., Yuan, Z., Hao, Z., Bai, X., Wu, Y., and Liu, Y.: A daily gap-
803 free normalized difference vegetation index dataset from 1981 to 2023 in China, *Sci*
804 *Data*, 11, 527, <https://doi.org/10.1038/s41597-024-03364-3>, 2024a.

805 Li, X., Xu, X., Sonnenborg, T. O., Andreasen, M., and He, C.: Effect of ecological
806 restoration on evapotranspiration and water yield in the agro-pastoral ecotone in
807 northern China during 2000–2018, *Journal of Hydrology*, 638, 131531,
808 <https://doi.org/10.1016/j.jhydrol.2024.131531>, 2024b.

809 Liang, L., Han, Z., Chen, W., Li, J., Liang, M., and Shen, S.: The source, transport,
810 deposition and direct radiative effect of mineral dust over western China: A modeling

811 study of July 2022 with focus on the Tibetan Plateau, *Atmospheric Research*, 311,
812 107708, <https://doi.org/10.1016/j.atmosres.2024.107708>, 2024.

813 Liu, C., Feng, S., Zhang, Q., Hu, J., Ma, N., Ci, H., Kong, D., and Gu, X.: Critical
814 influence of vegetation response to rising CO₂ on runoff changes, *Science of The Total*
815 *Environment*, 906, 167717, <https://doi.org/10.1016/j.scitotenv.2023.167717>, 2024.

816 Liu, J., Zhang, Q., Singh, V. P., and Shi, P.: Contribution of multiple climatic variables
817 and human activities to streamflow changes across China, *Journal of Hydrology*, 545,
818 145–162, <https://doi.org/10.1016/j.jhydrol.2016.12.016>, 2017.

819 Ma, T., Wang, T., Yang, D., and Yang, S.: Impacts of vegetation restoration on water
820 resources and carbon sequestration in the mountainous area of Haihe River basin, China,
821 *Science of The Total Environment*, 869, 161724,
822 <https://doi.org/10.1016/j.scitotenv.2023.161724>, 2023.

823 Medlyn, B. E., Duursma, R. A., Eamus, D., Ellsworth, D. S., Prentice, I. C., Barton, C.
824 V. M., Crous, K. Y., De Angelis, P., Freeman, M., and Wingate, L.: Reconciling the
825 optimal and empirical approaches to modelling stomatal conductance: RECONCILING
826 OPTIMAL AND EMPIRICAL STOMATAL MODELS, *Global Change Biology*, 17,
827 2134–2144, <https://doi.org/10.1111/j.1365-2486.2010.02375.x>, 2011.

828 Montibeller, B., Marshall, M., Mander, Ü., and Uuemaa, E.: Increased carbon
829 assimilation and efficient water usage may not compensate for carbon loss in European
830 forests, *Commun Earth Environ*, 3, 194, <https://doi.org/10.1038/s43247-022-00535-1>,
831 2022.

832 Mu, S., Zhou, S., Chen, Y., Li, J., Ju, W., and Odeh, I. O. A.: Assessing the impact of
833 restoration-induced land conversion and management alternatives on net primary
834 productivity in Inner Mongolian grassland, China, *Global and Planetary Change*, 108,
835 29–41, <https://doi.org/10.1016/j.gloplacha.2013.06.007>, 2013.

836 Nkiaka, E., Bryant, R. G., and Dembélé, M.: Quantifying Sahel Runoff Sensitivity to
837 Climate Variability, Soil Moisture and Vegetation Changes Using Analytical Methods,
838 *Earth Syst Environ*, 9, 491–504, <https://doi.org/10.1007/s41748-024-00464-3>, 2025.

839 Ogotu, B. O., D’Adamo, F., and Dash, J.: Impact of vegetation greening on carbon and
840 water cycle in the African Sahel-Sudano-Guinean region, *Global and Planetary Change*,
841 202, 103524, <https://doi.org/10.1016/j.gloplacha.2021.103524>, 2021.

842 Peng, H., Tague, C., and Jia, Y.: Evaluating the eco-hydrologic impacts of reforestation
843 in the Loess Plateau, China, using an eco-hydrologic model, *Ecohydrology*, 9, 498–513,
844 <https://doi.org/10.1002/eco.1652>, 2016.

- 845 Piao, S., Friedlingstein, P., Ciais, P., De Noblet-Ducoudré, N., Labat, D., and Zaehle,
846 S.: Changes in climate and land use have a larger direct impact than rising CO₂ on
847 global river runoff trends, *Proc. Natl. Acad. Sci. U.S.A.*, 104, 15242–15247,
848 <https://doi.org/10.1073/pnas.0707213104>, 2007.
- 849 Rahman, G., Farooq, U., Jung, M.-K., and Kwon, H.-H.: Spatiotemporal vegetation
850 dynamics in South Asia (2001-2023): roles of climate and anthropogenic activities,
851 *Geosci. Lett.*, 12, 31, <https://doi.org/10.1186/s40562-025-00403-8>, 2025.
- 852 Running, S. W., Thornton, P. E., Nemani, R., and Glassy, J. M.: Global Terrestrial
853 Gross and Net Primary Productivity from the Earth Observing System, in: *Methods in*
854 *Ecosystem Science*, edited by: Sala, O. E., Jackson, R. B., Mooney, H. A., and Howarth,
855 R. W., Springer New York, New York, NY, 44–57, [https://doi.org/10.1007/978-1-](https://doi.org/10.1007/978-1-4612-1224-9_4)
856 [4612-1224-9_4](https://doi.org/10.1007/978-1-4612-1224-9_4), 2000.
- 857 Serrano-Notivoli, R., Martínez-Salvador, A., García-Lorenzo, R., Espín-Sánchez, D.,
858 and Conesa-García, C.: Rainfall–runoff relationships at event scale in western
859 Mediterranean ephemeral streams, *Hydrol. Earth Syst. Sci.*, 26, 1243–1260,
860 <https://doi.org/10.5194/hess-26-1243-2022>, 2022.
- 861 Shen, Q., Cong, Z., and Lei, H.: Evaluating the impact of climate and underlying
862 surface change on runoff within the Budyko framework: A study across 224 catchments
863 in China, *Journal of Hydrology*, 554, 251–262,
864 <https://doi.org/10.1016/j.jhydrol.2017.09.023>, 2017.
- 865 Sims, D. A., Rahman, A. F., Cordova, V. D., Baldocchi, D. D., Flanagan, L. B.,
866 Goldstein, A. H., Hollinger, D. Y., Misson, L., Monson, R. K., Schmid, H. P., Wofsy,
867 S. C., and Xu, L.: Midday values of gross CO₂ flux and light use efficiency during
868 satellite overpasses can be used to directly estimate eight-day mean flux, *Agricultural*
869 *and Forest Meteorology*, 131, 1–12, <https://doi.org/10.1016/j.agrformet.2005.04.006>,
870 2005.
- 871 Sun, W., Ding, X., Su, J., Mu, X., Zhang, Y., Gao, P., and Zhao, G.: Land use and cover
872 changes on the Loess Plateau: A comparison of six global or national land use and cover
873 datasets, *Land Use Policy*, 119, 106165,
874 <https://doi.org/10.1016/j.landusepol.2022.106165>, 2022.
- 875 Sun, X., Dong, Q., and Zhang, X.: Attribution analysis of runoff change based on
876 Budyko-type model with time-varying parameters for the Lhasa River Basin, Qinghai–
877 Tibet Plateau, *Journal of Hydrology: Regional Studies*, 48, 101469,
878 <https://doi.org/10.1016/j.ejrh.2023.101469>, 2023.
- 879 Tan, X., Tan, X., Liu, B., and Huang, Z.: Contribution of changes in vegetation
880 composition and climate variability on streamflow across the global watersheds,
881 *CATENA*, 232, 107394, <https://doi.org/10.1016/j.catena.2023.107394>, 2023.

882 Tan, X., Jia, Y., Yang, D., Niu, C., and Hao, C.: Impact ways and their contributions to
883 vegetation-induced runoff changes in the Loess Plateau, *Journal of Hydrology:*
884 *Regional Studies*, 51, 101630, <https://doi.org/10.1016/j.ejrh.2023.101630>, 2024.

885 Wang, D. L., Feng, H. M., Zhang, B. Z., Wei, Z., and Tian, Y. L.: Quantifying the
886 impacts of climate change and vegetation change on decreased runoff in china's yellow
887 river basin, *Ecohydrology & Hydrobiology*, 22, 310–322,
888 <https://doi.org/10.1016/j.ecohyd.2021.10.002>, 2022.

889 Wasko, C. and Sharma, A.: Global assessment of flood and storm extremes with
890 increased temperatures, *Sci Rep*, 7, 7945, <https://doi.org/10.1038/s41598-017-08481-1>,
891 2017.

892 Wei, H., Zhang, Y., Huang, Q., Chiew, F. H. S., Luan, J., Xia, J., and Liu, C.: Direct
893 vegetation response to recent CO₂ rise shows limited effect on global streamflow, *Nat*
894 *Commun*, 15, 9423, <https://doi.org/10.1038/s41467-024-53879-x>, 2024.

895 Xiao, M., Gao, M., Vogel, R. M., and Lettenmaier, D. P.: Runoff and
896 Evapotranspiration Elasticities in the Western United States: Are They Consistent With
897 Dooge's Complementary Relationship?, *Water Resources Research*, 56,
898 e2019WR026719, <https://doi.org/10.1029/2019WR026719>, 2020.

899 Xu, X., Yang, D., Yang, H., and Lei, H.: Attribution analysis based on the Budyko
900 hypothesis for detecting the dominant cause of runoff decline in Haihe basin, *Journal*
901 *of Hydrology*, 510, 530–540, <https://doi.org/10.1016/j.jhydrol.2013.12.052>, 2014.

902 Xu, Z., Jiang, Y., Jia, B., and Zhou, G.: Elevated-CO₂ Response of Stomata and Its
903 Dependence on Environmental Factors, *Front. Plant Sci.*, 7,
904 <https://doi.org/10.3389/fpls.2016.00657>, 2016.

905 Xue, B., A, Y., Wang, G., Helman, D., Sun, G., Tao, S., Liu, T., Yan, D., Zhao, T.,
906 Zhang, H., Chen, L., Sun, W., and Xiao, J.: Divergent Hydrological Responses to Forest
907 Expansion in Dry and Wet Basins of China: Implications for Future Afforestation
908 Planning, *Water Resources Research*, 58, e2021WR031856,
909 <https://doi.org/10.1029/2021WR031856>, 2022.

910 Yang, H. and Yang, D.: Derivation of climate elasticity of runoff to assess the effects
911 of climate change on annual runoff: DERIVATION OF CLIMATE ELASTICITY OF
912 RUNOFF, *Water Resour. Res.*, 47, <https://doi.org/10.1029/2010WR009287>, 2011.

913 Yang, H. and Yang, D.: Climatic factors influencing changing pan evaporation across
914 China from 1961 to 2001, *Journal of Hydrology*, 414–415, 184–193,
915 <https://doi.org/10.1016/j.jhydrol.2011.10.043>, 2012.

- 916 Yang, H., Xu, H., Huntingford, C., Ciais, P., and Piao, S.: Strong direct and indirect
917 influences of climate change on water yield confirmed by the Budyko framework,
918 *Geography and Sustainability*, 2, 281–287,
919 <https://doi.org/10.1016/j.geosus.2021.11.001>, 2021.
- 920 Yang, L., Zhao, G., Tian, P., Mu, X., Tian, X., Feng, J., and Bai, Y.: Runoff changes in
921 the major river basins of China and their responses to potential driving forces, *Journal*
922 *of Hydrology*, 607, 127536, <https://doi.org/10.1016/j.jhydrol.2022.127536>, 2022.
- 923 Yang, Y., Xiao, P., Feng, X., and Li, H.: Accuracy assessment of seven global land
924 cover datasets over China, *ISPRS Journal of Photogrammetry and Remote Sensing*, 125,
925 156–173, <https://doi.org/10.1016/j.isprsjprs.2017.01.016>, 2017.
- 926 Yang, Y., Roderick, M. L., Zhang, S., McVicar, T. R., and Donohue, R. J.: Hydrologic
927 implications of vegetation response to elevated CO₂ in climate projections, *Nature*
928 *Clim Change*, 9, 44–48, <https://doi.org/10.1038/s41558-018-0361-0>, 2019.
- 929 Zeng, F., Ma, M.-G., Di, D.-R., and Shi, W.-Y.: Separating the Impacts of Climate
930 Change and Human Activities on Runoff: A Review of Method and Application, *Water*,
931 12, 2201, <https://doi.org/10.3390/w12082201>, 2020.
- 932 Zhai, R. and Tao, F.: Climate Change in China Affects Runoff and Terrestrial
933 Ecosystem Water Retention More Than Changes in Leaf Area Index and Land
934 Use/Cover Over the Period 1982–2015, *JGR Biogeosciences*, 126, e2020JG005902,
935 <https://doi.org/10.1029/2020JG005902>, 2021.
- 936 Zhang, B., Tian, L., Zhao, X., and Wu, P.: Feedbacks between vegetation restoration
937 and local precipitation over the Loess Plateau in China, *Sci. China Earth Sci.*, 64, 920–
938 931, <https://doi.org/10.1007/s11430-020-9751-8>, 2021a.
- 939 Zhang C., WU C., KUAIS., PENG Z., Chang R., and ZHANG S.: Water-heat coupling
940 model-based study on runoff driving mechanism of Zhenjiangguan Watershed, *Water*
941 *Resources and Hydropower Engineering*, 53, 78–87,
942 <https://doi.org/10.13928/j.cnki.wrahe.2022.08.008>, 2022a.
- 943 Zhang, J., Zhang, Y., Sun, G., Song, C., Dannenberg, M. P., Li, J., Liu, N., Zhang, K.,
944 Zhang, Q., and Hao, L.: Vegetation greening weakened the capacity of water supply to
945 China’s South-to-North Water Diversion Project, *Hydrol. Earth Syst. Sci.*, 25, 5623–
946 5640, <https://doi.org/10.5194/hess-25-5623-2021>, 2021b.
- 947 Zhang, J., Zhang, Y., Sun, G., Song, C., Li, J., Hao, L., and Liu, N.: Climate Variability
948 Masked Greening Effects on Water Yield in the Yangtze River Basin During 2001–
949 2018, *Water Resources Research*, 58, e2021WR030382,
950 <https://doi.org/10.1029/2021WR030382>, 2022b.

951 Zhang, S., Yang, H., Yang, D., and Jayawardena, A. W.: Quantifying the effect of
952 vegetation change on the regional water balance within the Budyko framework,
953 Geophysical Research Letters, 43, 1140–1148, <https://doi.org/10.1002/2015GL066952>,
954 2016a.

955 Zhang, X., Zhao, T., Xu, H., Liu, W., Wang, J., Chen, X., and Liu, L.: GLC_FCS30D:
956 the first global 30 m land-cover dynamics monitoring product with a fine classification
957 system for the period from 1985 to 2022 generated using dense-time-series Landsat
958 imagery and the continuous change-detection method, Earth Syst. Sci. Data, 16, 1353–
959 1381, <https://doi.org/10.5194/essd-16-1353-2024>, 2024.

960 Zhang, Y., Song, C., Sun, G., Band, L. E., McNulty, S., Noormets, A., Zhang, Q., and
961 Zhang, Z.: Development of a coupled carbon and water model for estimating global
962 gross primary productivity and evapotranspiration based on eddy flux and remote
963 sensing data, Agricultural and Forest Meteorology, 223, 116–131,
964 <https://doi.org/10.1016/j.agrformet.2016.04.003>, 2016b.

965 Zhao, F., Wu, Y., Ma, S., Lei, X., and Liao, W.: Increased Water Use Efficiency in
966 China and Its Drivers During 2000–2016, Ecosystems, 25, 1476–1492,
967 <https://doi.org/10.1007/s10021-021-00727-4>, 2022.

968 Zhou, S., Yu, B., Huang, Y., and Wang, G.: The effect of vapor pressure deficit on
969 water use efficiency at the subdaily time scale, Geophysical Research Letters, 41, 5005–
970 5013, <https://doi.org/10.1002/2014GL060741>, 2014.

971 Zhou, S., Yu, B., Lintner, B. R., Findell, K. L., and Zhang, Y.: Projected increase in
972 global runoff dominated by land surface changes, Nat. Clim. Chang., 13, 442–449,
973 <https://doi.org/10.1038/s41558-023-01659-8>, 2023.

974
975